Chapter-6

Congo red disintegrating $MgNiAl-CO_3$ Layered double hydroxide (LDH) and its derivative having high recyclability

6.1. Abstract

In this study, both uncalcined and calcined $[Mg_{0.5}^{2+}Ni_{0.25}^{2+}Al_{0.25}^{3+}(OH)_2].(CO_3^{2-})_{0.125}.H_2O$ or MgNiAl-CO_3 layered double hydroxide was used as an adsorbent in the adsorption of Benzidinediazo-bis-1-naphthylamine-4-sulfonic acid; (Congo-red) from aqueous solution in the batch adsorption. The surface property of layered double oxide was improved by calcination at 500 °C for 4 h. X-ray diffraction, Fourier Infrared Spectroscopy, Scanning Electron Microscopy, Transmission Electron Microscopy and X-ray photoelectron spectroscopy were used to characterise the material. The role of different parameters, such as pH variation, adsorbent dosage, initial dye concentration, and reusability, were investigated. The adsorption kinetics were analysed using the pseudo-first order, pseudo-second order, and intraparticle diffusion models. The Langmuir and Freundlich isotherm models were used to analyse the equilibrium adsorption isotherm. These results demonstrated that the Langmuir isotherm model fitted the experimental data with a high correlation coefficient. The maximum adsorption capacity was calculated at 181.81 and 480.76 mg/g for uncalcined and calcined Layered double hydroxide. The calcined material was highly stable, showing remarkable reusability up to the 14th cycle. These results suggest that the prepared material is a very efficient adsorbent for dye removal from textile industries' wastewater.

6.2. Results and discussion

6.2.1. Characterisation

6.2.1.1. X-ray diffraction of MgNiAl-CO_3 LDH and calcined MgNiAl-CO_3 LDH*:*

The X-ray diffraction pattern of the $MgNiAl-CO_3$ and calcined LDH and calcined LDH after CR adsorption are shown in Figure. 6.1a. In Figure. 1(a-i), the series of peaks (003), (006), (012), and (110) were located at 11.35°, 22.94°, 34.54°, and 60.57° appeared in LDH as symmetric diffraction peaks, these might indicate that LDH possessed hydrotalcite and well order layered structure. The sharp peaks indicate that the LDH is highly crystalline. Furthermore, the series of peaks (012), (015), (018), (110), and (113) proved that LDH had a hexagonal lattice, which was due to the

presence of anion in the interlayer [219,220]. The XRD pattern of calcined LDH is shown in Figure 6.1.(a-ii); after 4 h of calcination at 500 °C, the layered structure was destroyed. Only two broad peaks remain after calcination, indicating that the structure was destroyed by the elimination of the water molecules and interlayer anion [232,233]. In the spectrum, metal oxides like MgO, NiO, and MgO/NiO can be seen as they form.

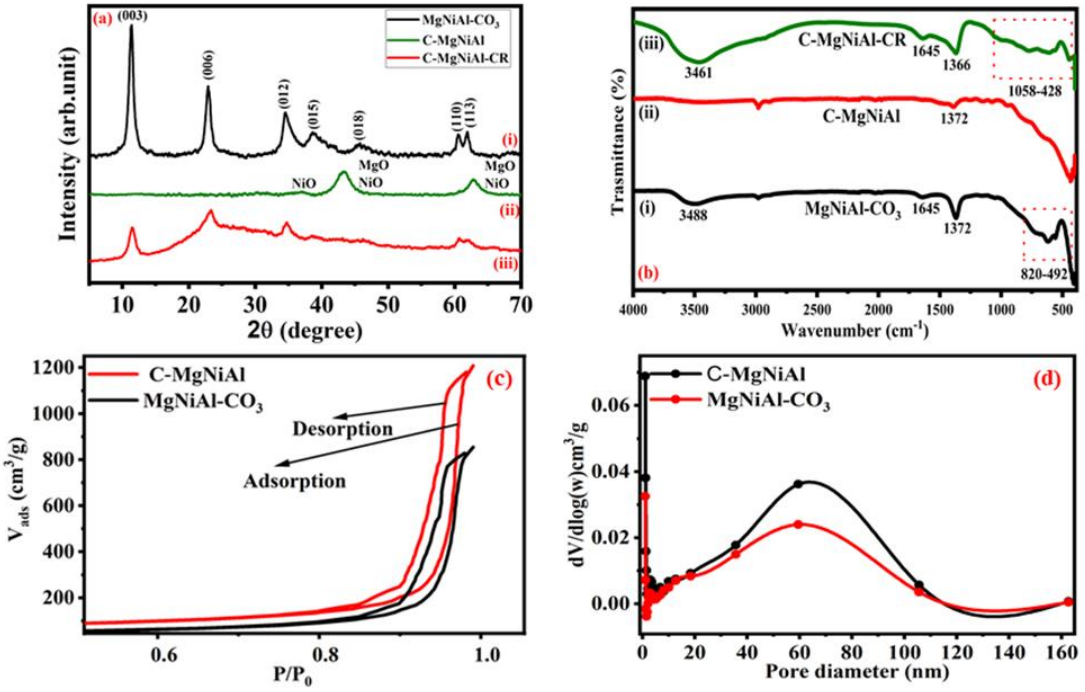

Figure 6.1: X-ray diffraction pattern of (a-i) $MgNiAl - CO_3$ LDH (a-ii) $C - MgNiAl$ and (a-iii) $C - MgNiAl$ after CR adsorption. FTIR spectra of uncalcined LDH (b-i) Unalcined LDH (b-ii) calcined LDH (b-iii) Calcined LDH after adsorption of CR. (c) Nirogen adsorption-desorption isotherm of both calcined and uncalcined LDHs (d), pore size distribution of calcined and uncalcined LDH.

The low crystallisation temperature prevents the presence of comparable peaks of aluminum oxide [234]. X-ray diffraction of calcined LDH after CR adsorption is shown in Figure. 6.1(a-iii). Compared to the LDH, this spectrum shows the same initial peaks at a lesser intensity. The same observations were reported by other authors like Ferreira et al, Boudief et al [234,235]. This is caused by calcined LDH reconstructing the layered structure following CR adsorption; the majority interlayered anion, OH^- originates from CR, while the intercalated anion, CO_3, originates from the surrounding air medium [233,234].

6.2.1.2. Fourier Transform Infrared (FTIR) Spectrum

The FTIR spectrum of uncalcined, calcined, and after CR adsorption by calcined LDH is shown in Figure 6.1b. This Figure displays adsorption spectra of stretching and bending vibration of hydroxyl bond due to interlayered anion and water molecules present in between stacking layered and stretching vibration bond of metal-oxygen-metal [234,236,237]. The broad, and highly intense band observed around 3488 cm^{-1} ascribed the $O-H$ ions due to water molecules present in the materials and $O-H$ bond connected with cations. This band becomes less intense due to the calcination of LDH at high temperatures, as shown in Figure (b-ii). The less intense band was observed at 1645 cm^{-1} due to the bending vibration of deformation ($\delta(H_2O)$) water molecules present in the material [238]. The strong band at 1367 cm^{-1} slightly shifted to 1388 cm^{-1} and became weaker in $C-MgNiAl$ due to calcination, indicating the asymmetric stretching vibration of interlayer CO_3 anion. This band becomes weak and slighty shifts due to calcination, but it does not vanish. It suggests that some interlayer anion remains, and is completely removed when the LDH is calcined at a high temperature around or greater than 700 °C, which was observed in the literature [238,239]. The band in the lower frequency range 500 to 1000 cm^{-1} defines the formation of lattice vibration mode of $M-O,\ M-OH, M-O-M$ ($M = Mg, Ni\ and\ Al$) [240,241]. The FTIR spectra of calcined LDH after CR adsorption is shown in Figure 6. (b-iii). The FTIR spectrum of after CR adsorption, broad band near around 3461 cm^{-1} is coming due to $O-H$ stretching vibration band. The band near around 1645 cm^{-1} represents the $N=N$ stretching vibration of the azo group. The band near at 1366 cm^{-1} and 1058 cm^{-1} corresponds to $C-N$ and $S=O$ stretching vibration of CR dye respectively [242,243]. This finding demonstrated that calcined LDH is involved for CR adsorption.

6.2.1.3. Nitrogen adsorption-desorption isotherm

The N_2 adsorption-desorption isotherm of calcined, uncalcined LDH and their pore size distribution curve are shown in Figure 6. 1(c & d). This material displays type V isotherms, which are unusual and connected to type III isotherms, according to the earlier study; in this instance, the interaction between the adsorbent and adsorbate is extremely weak. This isotherm displays an H1-type hysteresis at high relative pressure, characteristic of compacts or agglomerates of uniformly shaped spheres arranged in a

regular pattern, and hence a narrow distribution of pore size [244]. This type of shape is typical with porous materials, which quickly diffuse any reactance through these large pores. According to the data in Figure. 6.1d, both materials' pore size distribution (PSD) curves are pointed and have a porous quality. The peak position of the two PSD curves is the same for both materials small peaks centred at $4-6$ nm and broad peaks centred at 59 nm. This observation confirmed the presence of mesopores and macropores [245,246]. Larger mesopores remain with pores created between the stacked nanosheet, whereas smaller mesopores are the reflected pores that remain inside nanopores [246]. This class of porous materials is crucial as an adsorbent for the anionic dye molecules used in the textile industry. The materials can be used in the adsorption process, even with adsorbents ranging from 5 to 20 Å [247].

In Table 6.1, the material's textural characteristics are listed. The specific surface area of $MgNiAl-CO_3$ increased from 132 $^{m^2}/_{g}$ to 218 $^{m^2}/_{g}$, and pore volumes are 1.31 cm^3/g to 1.85 cm^3/g by the heating at 500 °C for 4 h. Mean pore size was determined by the ratio between the mesopores volume (V_{mp}), and specific surface area (S_{BET}), $3.5V_{mp}/S_{BET}$. The surface area and pore volume of calcined LDH are more significant than LDH, but the mean pore diameter size is decreased. That is the removal of intercalated anion and water molecules by calcination temperature, which can ensure the formation of channels and pores, increasing the specific surface area and pore volume [248,249].

Table 6.1: Experimental textural properties of the samples.

Sample	Surface area ($^{m^2}/_{g}$)	Average pore diameter (nm)	Pore volume ($^{cm^3}/_{g}$)
$MgNiAl-CO_3$	132	34.24	1.31
$C-MgNiAl$	218	28.35	1.85

6.2.1.4. Morphology, and element composition

The surface morphology of the LDH has been studied through SEM, and TEM analysis is shown in Figure 6.2. SEM measurements demonstrated that the surface of LDH has an uneven size and correct hexagonal form morphology but overlaps each other as shown in these images [250,251].

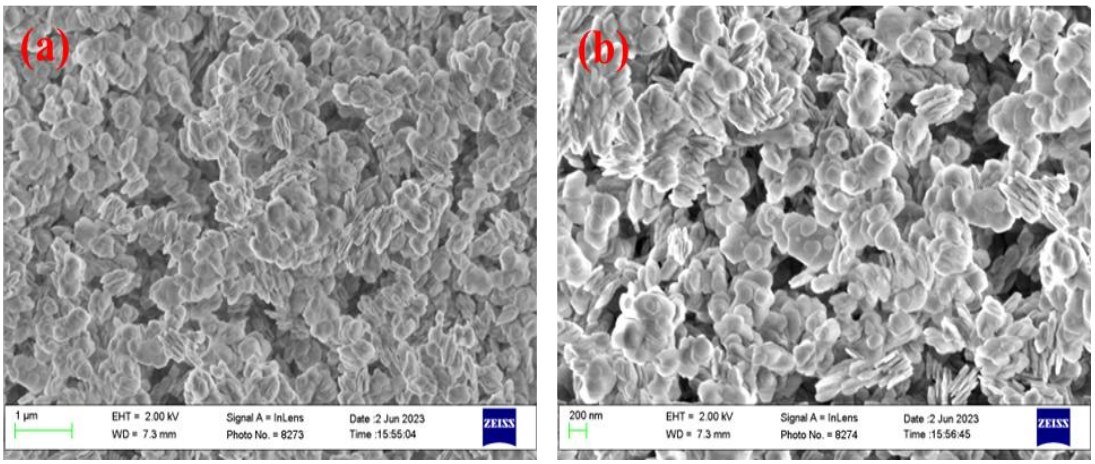

Figure 6.2: SEM images of MgNiAl-CO_3 layered double hydroxide at different magnification.

6.2.2. Kinetic Studies

6.2.2.1. The effect of solution pH

The pH of the dye solution is one of the most important variables in the adsorption process. The impact of pH on CR adsorption on the surface of LDH and calcined LDH was illustrated in Figure. 6.3a. The effectiveness of dye removal is lower at pH 4.0 and pH 10 than pH 7.0. The maximum adsorption capacity is 18.6 $\pm$ 0.5 mg/g at pH 4, 19 $\pm$ 0.5 mg/g at pH 7 and 16.5 $\pm$ 1 mg/g at pH 10. The adsorption capacity decreases at pH 4 and 10, showing maximum adsorption at pH 7. This could be understood from the charge of the material and dye at different pH, which is confirmed through the Zeta potential analysis, shown in Figure 6.3b. Under the acidic and alkanine medium the negative value of the Zeta potential of the dye is less than normal medium. On the other hand, the positive Zeta potential of the material at normal pH is greater than the acidic and alkaline medium. So, the electrostatic attraction force between the adsorbate and adsorbent at normal pH is greater than in acidic and alkaline mediums, which increases the adsorption capacity of the material. The Zeta potential value of the material and dye at normal pH is 30.1 and -68.3 mV, which makes the stability of the material.

6.2.2.2. Effect of contact time on Congo-red removal

The rapid increase in CR adsorption throughout the first 10 minutes for both samples is shown in Figure 6.3c. In the same conditions, the adsorption process reached saturation at 40 minutes for LDH, and 90 minutes for calcined LDH. The CR anions adsorption on the surface, and the ion exchange phenomena caused by reconstruction (memory effect) can be utilised to clarify why it takes more time to achieve equilibrium conditions for saturation processes. Utilising the calcination process, adsorbate containing water, and anion species can be used to recreate layered structures. The CR anions diffused in the LDH's interlayers in this instance, and saturations required a very

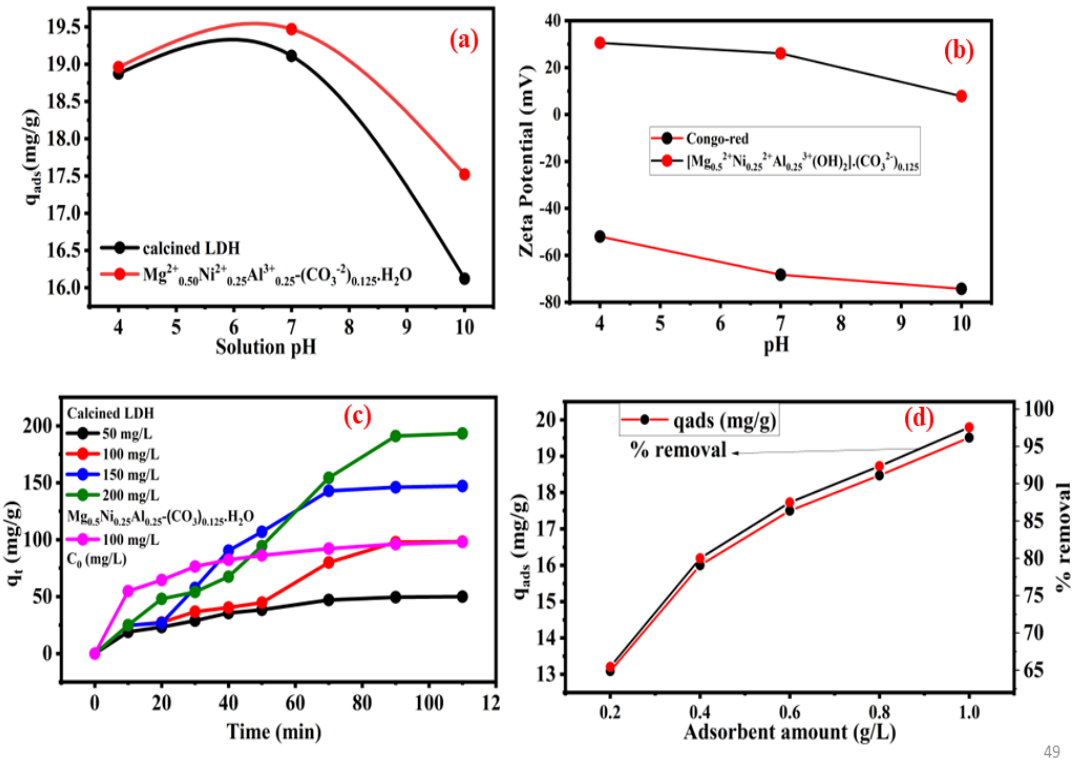

Figure 6.3: (a) Effect of pH in adsorption of CR on the two sample (V_{sol} = 25 ml, adsorbent mass = 25 mg, C_0 = 20 mg/L. (b) Zeta Potential (c) Effect of time and initial concentration in the adsorption of CR on the two sample (V_{sol} = 50 ml, adsorbent mass = 50 mg. (d) effect of adsorbent amount for adsorption.

long time to achieve. On the other hand, because the outer surface carbonated ions on the surface of LDH are weakly bound compared to the intercalated anions and are easily replaced by CR, the adsorption process of CR on the surface of LDH proceeds extremely slow. As a result, the adsorption rate becomes slower than the initial rate.

This Figure also demonstrates that, under identical conditions, calcined LDH consumed more dye than LDH [234].

6.2.2.3. Effect of congo-red (CR) Concentration

The initial concentration of CR significantly influences the efficiency of the adsorption process by the LDH and calcined LDH. The amount of CR adsorbed by calcined LDH was 49.36 mg/g to 193.26 mg/g as shown in Table 6.2 and Figure 6.3c (time vs q_t), it shows the calculated removal efficiency % decreased in this case very small 98.7 % to 96.6 % with increasing the amount of CR concentration 50 mg /L to 200 mg/L. Due to the existence of more active sites on the adsorbent surface, there was a higher absorption at low concentrations. At an initial higher concentration of CR, the ratio of the initial mole number of CR to surface area is high; as a result, the removal % becomes less than at a lower concentration. Increase the concentration of the adsorbate such that the % removal efficiency of CR becomes reduced [252].

6.2.2.4 Effect of adsorbent dosage

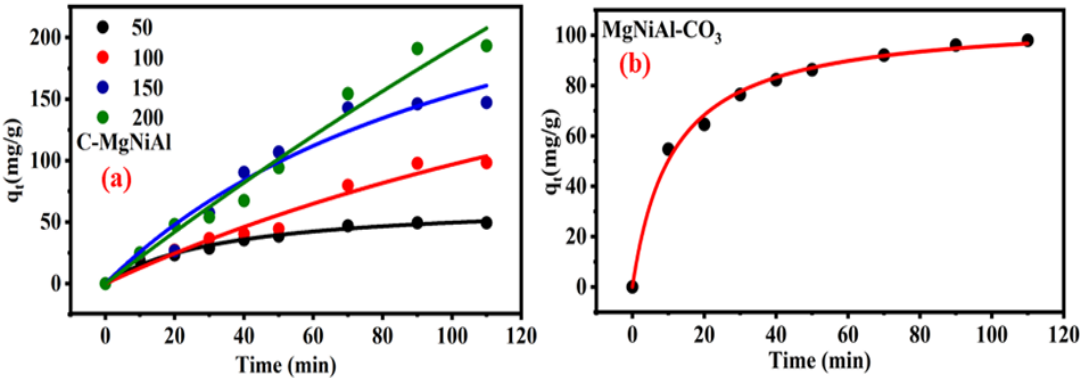

Figure 6.4: (a) Pseudo-second order kinetics for adsorption of congo-red on the $C-MgNiAl$ LDH and (b) $MgNiAl-CO_3$ LDH, dot represents the experimental data and line indicates the fitting data (V_{sol} =50 ml, adsorbent mass = 50 mg.)

The removal effectiveness of congo-red was directly impacted by the amount of the C − MgNiAl, shown in Figure 6.3d. As previously discussed, with increasing adsorbate concentrations, the availability of higher energy sites may be reduced as a significant portion of sites with lower energy become occupied, resulting in a lower adsorption capacity; this Figure discusses maximum adsorption capacity [253]. This Figure shows that with vary of the amount of adsorbent dosage from 0.2 to 1 g/L, the percentage of

CR removal increased from 65.45% to 97.55% for 20 mg/L solution concentration. At low concentrations of adsorbate, there is a higher adsorption efficiency. All types of active adsorbent surface sites are fully exposed at low adsorbent concentrations, which helps the surface reach saturation more quickly and results in a larger adsorption capacity [253,254]. The concentration of CR was fixed to verify the removal effectiveness depending on the ratio of the number of CR moles to the accessible surface area of the adsorbent. Adsorbate concentration was maintained at a specific concentration while removal effectiveness was compared. The percentage of adsorbate removal was increased because of the amount of adsorbent. Additionally, the likelihood of interactions between solid molecules is increased in higher adsorbents, causing particles to aggregate with one another, reduce surface area, and lengthen diffusion paths, decreasing the effectiveness of CR removal [254].

6.2.3. Kinetics model of Congo-red adsorption onto the uncalcined and calcined layered double hydroxide

To construct and optimise the adsorption kinetic system, it is essential to study the adsorption effectiveness of an adsorbent using its adsorption kinetics. Pseudo-first-order, pseudo-second-order, and intraparticle diffusion models are designed and fitted here to explore the control mechanism system of the adsorption process, including chemical reaction, diffusion control, and mass transfer. The experimental results from the CR adsorption onto the LDH and calcined LDH are fitted by these models. The kinetics of CR adsorption onto LDH and calcined LDH were analysed by the pseudo-first-order kinetic model expressed by the following equation (3)

$$\ln(q_e - q_t) = lnq_e - k_1 t \dots\dots\dots\dots\dots\dots\dots\dots\dots\dots\dots\dots\dots\dots\dots\dots\dots\dots\dots\dots\dots\dots (3)$$

and pseudo-second-order kinetic model expressed by the equation (4)

$$q_t = q_e^2 . k_2 . t/(1 + q_e . k_2 . t) \dots\dots\dots\dots\dots\dots\dots\dots\dots\dots\dots\dots\dots\dots\dots\dots\dots\dots\dots\dots\dots\dots (4)$$

The correlation coefficient R^2 expresses the consistency between the experimental and model-predicted values. The pseudo-first-order and pseudo-second-order kinetic model's adsorption rate constants are k_1, k_2, and q_e as well as the correlation coefficient, which are shown in Table 6.2.

Table 6.2: kinetic models parameters obtained in adsorption of congo red on uncalcined and calcined MgNiAl-CO_3 layered double hydroxide pseudo-first-order and pseudo-second-order.

C_0	$q_{e,exp}$	Pseudo-second order			Pseudo-first order		
		$q_{2,cal}$	k_2 (10^{-5})	R^2	$q_{1,cal}$	k_1 (10^{-4})	R^2
$C - MgNiAl$							
50	49.36	66.42 ± 3.95	44.2	0.985	117.59±0.54	-5.1	0.873
100	98.36	361.14±198.69	2.34	0.953	274.71±0.50	-4.5	0.866
150	147.13	755.13±96.08	1.01	0.954	342.02±0.26	-47.5	0.952
200	193.26	1624.05±1867.13	0.082	0.972	548.44±0.42	-43.6	0.894
$MgNiAl - CO_3$							
100	97.92	106.49±2.24	83.9	0.994	94.51±0.283	-42.6	0.94

C_0(mg/L), m (mg), T(K), q_e (mg/g), k_1 (min^{-1}), k_2 (g $(mg.min)^{-1}$)

The non-linear form of pseudo-second-order (plot $q_t\ vs\ t$), and linear form of pseudo-first-order kinetic model form of ln $(q_e - q_t)$, and time t for adsorption of congo-red onto the calcined LDH and LDH are shown in Figure 6.4 and Figure 6.5 respectively. As shown in Table 6.2, the rate constant of the pseudo-first-order decreased from $-5.1\ to\ -43.6\ \mathrm{min}^{-1}$, and the rate of pseudo-second-order decreased from 4.4×10^{-4} to $8.82 \times 10^{-7}\ \mathrm{min}^{-1}$ with an increase in concentration from 50 to 200 mg/L. The value of q_e increased sharply (Table 6.2) demonstrated that the correlation coefficient R^2 of the pseudo-second-order model greater than the pseudo-first-order kinetic model. So pseudo-second-order kinetic model is suitably fitted. Therefore, it is appropriate to discuss the mechanism of the adsorption process of CR onto calcined LDH, and LDH using the pseudo-second-order kinetic model. The surface solid phase and chemisorption mechanism by materials are described by the pseudo-second-order kinetic model. This result also matches with previous literature [255]. The ability to discuss the entire adsorption process is another benefit of the pseudo-second-order kinetic model.

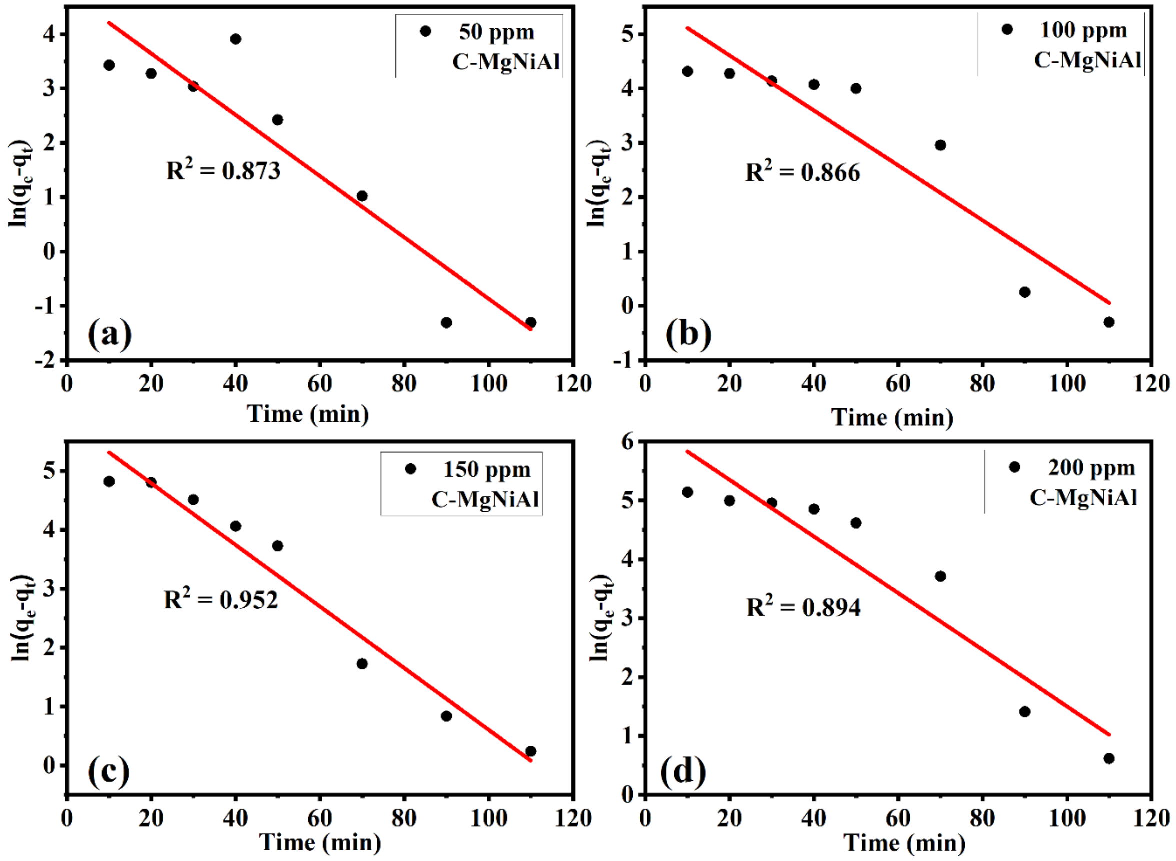

Figure 6.5: Pseudo-first-order kinetic model for calcined MgNiAl-CO_3 LDH, dot indicates the experimental value and line represents the liner fitting (model is not suitable for lower R^2, ppm = mg/L).

The intraparticle mass transfer model was suggested by Weber, and Morris to specify the diffusion mechanism in the adsorption of CR onto the calcined LDH.

$$q_t = k_i t^{1/2} + C \quad \ldots\ldots\ldots\ldots\ldots\ldots\ldots\ldots\ldots\ldots\ldots \text{(5)}$$

In this equation (5), C (mg/g) is the intercept, and k_i (mg/g. $min^{1/2}$) is the intraparticle diffusion model rate constant. The plot q_t vs $t^{1/2}$ gives the straight line as shown in Figure 6.6 (SI). The value of C, and the rate constant k_i is calculated from the intercept and slope of the straight line. The information about layer thickness and boundary is

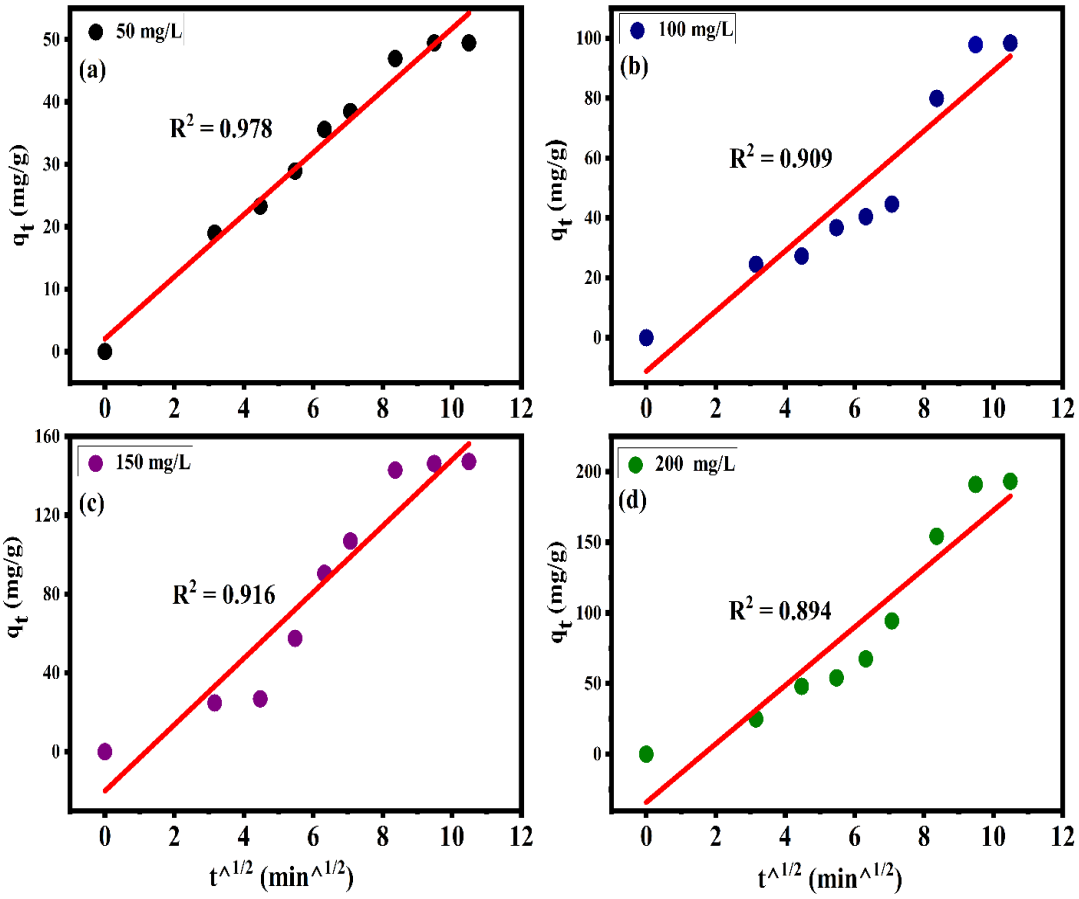

Figure 6.6: Intraparticle diffusion model for CR adsorption onto the calcined MgNiAl-CO_3 LDH, dot indicate experimental value and red line represent the linear fitting.

given by the intercept and slope values. It was found that the diffusion rate constant increased from 4.97 to 20.65 mg/g.$min^{1/2}$ and intercept decrease from 2.02 to $-$ 33.95 mg/g with an increase of CR concentration from 50 mg/L to 200 mg/L. These findings show that increasing the CR concentration content seems to increase the rate of CR diffusion in the boundary layer and enhance solid-state diffusion.

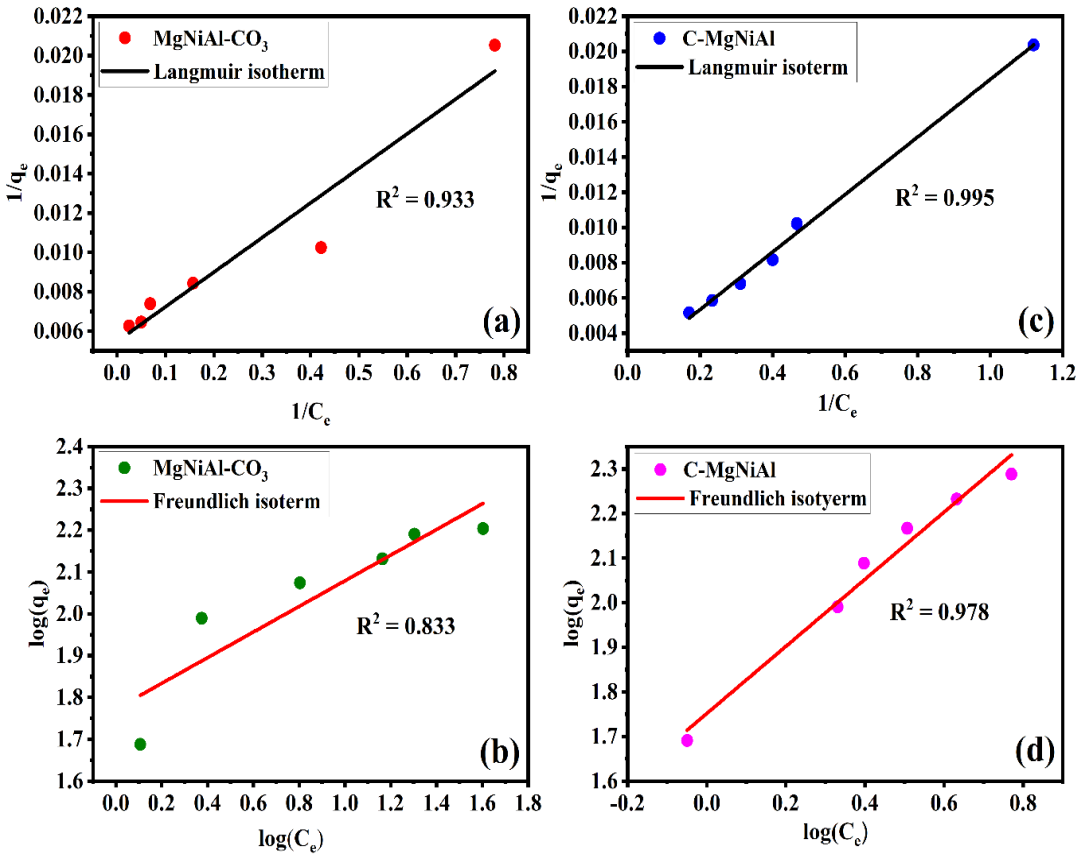

Figure 6.7: Langmuir and Freundlich isotherm model fit for CR adsorption by MgNiAl-CO_3 LDH (a & b). and by C-MgNiAl (c & d). by C-MgNiAl LDH, dot indicate the experimental value and line indicate the linear fitting. (V_{sol} =50 ml, adsorbent mass = 50 mg). (R^2 of Langmuir isotherm is greater than R^2 of Freundlich isotherm).

6.2.4. Equilibrium Adsorption Isotherms

For solid-liquid systems, the equilibrium of adsorption is one of the most important isotherms to define how much adsorbate is adsorbed on the adsorbent surface. The phenomenon of adsorption isotherm has been clarified using batch experiments at different adsorbate concentrations. Langmuir and Freundlich, two well-known models, are discussed in this work. Numerous factors obtained from different fitted models are used to explain the adsorption mechanism, surface characteristics, and affinity of the adsorbate to the adsorbent. The Langmuir isotherm model proposes that the energy of adsorption is constant and there are a certain number of adsorbent sites that are

constantly available on the adsorbent surfaces, each of which is occupied by a single monolayer molecule.

$$\frac{1}{q_e} = \frac{1}{(q_m \times K_L \times C_e)} + \frac{1}{q_m} \ldots\ldots\ldots\ldots\ldots\ldots\ldots\ldots\ldots\ldots\ldots \quad (6)$$

or,

$$\frac{C_e}{q_e} = \frac{1}{(K_L \times q_m)} + \frac{C_e}{q_m}$$

The maximum adsorption (q_m) was calculated from the Langmuir isotherm model, correlating to the whole monolayer coverage on the adsorbent surface. The adsorption isotherm of CR adsorbed by LDH and calcined LDH is shown in Figure 6.7. Plotting the curve $\frac{1}{q_e}$ vs $\frac{1}{C_e}$, which gives the maximum adsorption capacity as well as the Langmuir constant, which relates to the energy of the adsorption, yields the maximum adsorbent capacity (q_m). This isotherm shows that CR has a higher affinity for calcined LDH than LDH. The surface of LDH, CR has a positive and negative charge. Therefore, the adsorption process responds to the coulomb attraction force between them. Table 6.3 shows the result of the linear-fitted Langmuir and Freundlich models. The correlation coefficient R^2 of the Langmuir model is higher than the Freundlich model, indicating the sample surface's homogenous nature and CR's monolayer formation onto the LDH and calcined LDH surface. The amount of CR adsorbed by calcined LDH is greater than LDH at the same concentration. The maximum adsorption capacity by the calcined LDH is 480.76 mg/g, and 181.81 mg/g by uncalcined LDH; another adsorbent adsorbed a similar adsorbate was reported (Table 6.4). This difference happens with the increase in material surface area during the calcination process. The Freundlich isotherm model assumes that the adsorption surface becomes heterogeneous during the adsorption process. The Freundlich constant K_f, and n provides the adsorption process's approximate adsorption capacity and intensity, respectively. The Freundlich isotherm model is expressed by the equation (7).

$$\log(q_e) = \log(K_f) + \frac{1}{n}\log(C_e) \text{ or } q_e = K_f C_e^{1/n} \ldots\ldots\ldots\ldots\ldots \quad (7)$$

The curve plotted against $log q_e \ vs \ log C_e$ which gives the coefficient K_f, and n. Where K_f is related to the bonding energy, represents the quantity of dye adsorbed on the surface of the adsorbent unit equilibrium concentration, and defines the adsorption or

distribution coefficient. $\frac{1}{n}$ indicates the adsorption intensities of adsorbent or surface heterogeneity, which become more heterogeneity when $\frac{1}{n}$ value gets close to zero. The $\frac{1}{n}$ value greater than 1 indicates cooperative adsorption, and less than 1 indicates a normal Langmuir isotherm.

Table 6.3: Langmuir, Freundlich isotherm model constant and correlation coefficient for adsorption of Congo-red onto the prepared sample

Isotherm	$\mathbf{MgNiAl-CO_3}$	$\mathbf{C-MgNiAl}$
Langmuir	**q_m= 181.81 mg/g** K_L= 1 L/mg R^2= 0.933	**q_m= 480.76 mg/g** K_L= 0.127 L/mg R^2= 0.995
Freundlich	K_f = 2.024 mg/g n = 3.26 $1/n$= 0.306 R^2= 0.833	K_f = 56.42 mg/g n = 1.32 $1/n$= 0.752 R^2= 0.978

Table 6.4. Comparison of monolayer equilibrium capacity for CR with another adsorbent.

Adsorbent Name	$\mathbf{q_m(\frac{mg}{g})}$	References
Calcined MgNiAl-CO_3	**480.76**	**This study**
Ternary CaNiAl LDH	135.21	[256]
Binary Mg-Al LDH	111.11	[243]
Organo attapulgite	189.39	[257]
Shiitake Mushroom	217.86	[258]

6.2.5. Recycle Test

Its recyclability was also investigated to determine the stability of recurrent reactions over the calcined LDH sample. Due to its economic viability, recyclability has only been used for calcined LDH after dye adsorption. This process was tested with the 100 mg/L ($V_{sol} = 50\ ml, adsorbent\ mass = 50\ mg$) dye concentration. No significant

reduction of material activity was found, confirming that the material was very stable during the adsorption process, even after the 14th cycle. The adsorbent was collected after the adsorption experiments and can be reused following a thermal treatment at 500 °C for 4 h under an air medium. Apart from that, the material exhibits a previous structure equivalent to previously calcined material (Figure 6. 9a).

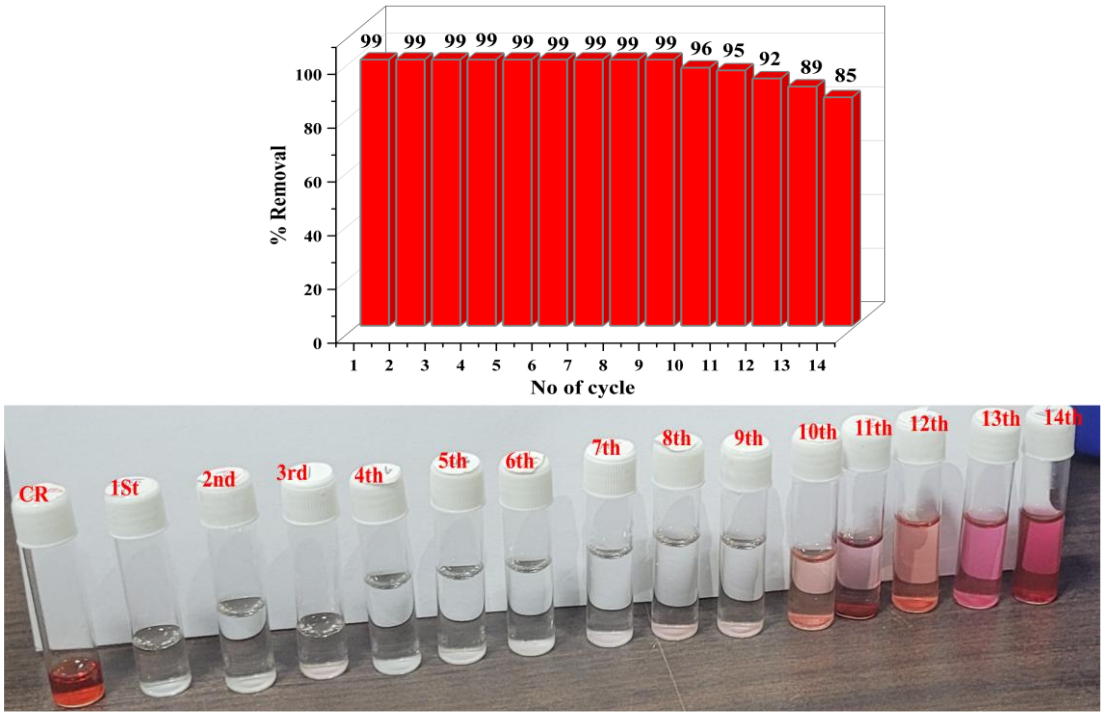

Figure 6.8: Recycle test by the C-MgNiAl LDH.

Jae-Hong Kim et al. reported that $Au/TiO_2/LDH$ reduced its efficiency after the 5th cycle due to its minimal morphological changes in composite materials [259]. Hibino and Tsunashima reported the repeated calcination of Mg-Al-LDH at 673 K. They claimed that Al was removed from the compound because of the calcined materials, significantly reducing performance [260]. The same material but Cl as an intercalated anion is calcined by Shin et al. for phosphorous removal. According to their findings, the material was subjected to anion exchange with carbonate after the phosphorus was adsorbed. After the 5th cycle, the material's performance declined [261]. Jairo Tronto et al. reported that the efficiency of calcined Mg-Al LDH for removing Acid Yellow 42 dye was reduced after the 5th cycle up to 62.5 % [262]. Eduardo L. Crepaldi et al. reported the adsorption of terephthalate by calcined hydrotalcite compounds [263]. They have reported after the 5th cycle, the efficiency of the adsorption capacity of the adsorbent reduced efficiently. E.E. Abdel-Hady et al. reported that Crystal violet

adsorption by Ternary Zn-Mg-Al LDH and its recycling reduced by 68.04 % within the 5th cycle [264].

In this case, the adsorption capacity of Congo-red after the 9th cycle was still 99 %; after the 9th cycle to the 14th, the efficiency of the material reduced to only 15 %, as shown in Figure 6.8. It will go a long cycle of up to 50 %, decreasing the efficiency of the material. The adsorption capacity of Congo-red by calcined LDH was tested up to the 14th cycle. In this case, the potential of calcined LDH to absorb CR following a slight and progressive decline in adsorption capacity demonstrates the material's effectiveness.

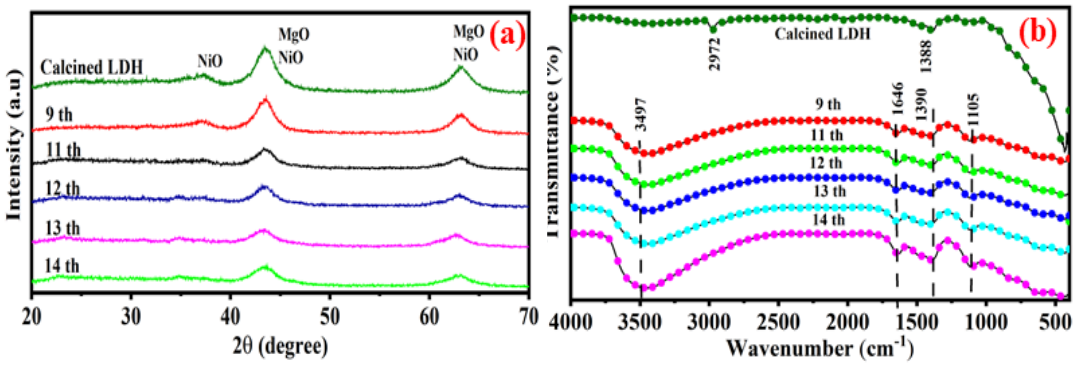

Figure 6.9: (a) X-ray diffraction pattern and (b) FTIR spectra of recycle materials.

6.2.5.1. Effect of crystallite size of regeneration materials

This section investigates the change in the crystallite size of the material that undergoes heat treatment for calcination. The material was calcined at 500 °C for 4 h in an air medium using a muffle furnace following each adsorption stage. X-ray diffraction was used to characterise the material and measure the crystallite size, as shown in Figure 6.9. This Figure shows that the XRD pattern remained unchanged; only the crystallinity changed. The crystallite sizes of the calcined materials' first and second high-intense peaks are 67 and 62 nm, with peak positions at 43.16° and 62.53°, respectively, and other materials' crystallite sizes are listed in Table 6.5. A progressive loss of crystallinity was seen for the adsorbed materials (Figure 6.9a) during the recycling, which is listed in Table 6.5. It can be concluded from Table 5 that the material's adsorption capacity might decrease with the crystallite size of the materials. The materials' decreased crystallinity nature prevents them from adsorption Congo Red.

Table 6.5. List of the crystallite size

Name of the recycled sample	The crystallite size of the first peak (nm, position near 2θ = 43°)	Crystallite size of second peak (nm, position near 2θ = 63°)
C − MgNiAl	**67**	**62**
9th	**65**	**61**
11th	**64**	**61**
12 th	**63**	**61**
13th	**63**	**61**
14th	**63**	**61**

6.2.5.2.Fourier transform infrared spectroscopy analysis

FTIR analysis of each material obtained after calcination in the different recycle tests, including calcined LDH before adsorption, is shown in Figure 6. 9b. A small hump around 2972 cm^{-1} can be due to the stretching vibration of the hydrogen bond between interlayer water and carbonate anion present in the interlayer. The peak around 1384 cm^{-1} indicating the asymmetric stretching vibration of interlayer CO_3 anion. After the adsorption of the CR dye, some new peak arises (up to the 9th to 14th cycle), and all peaks correspond to the new function group related to CR dye. As the number of recycling increased, this functional group had an impact on the adsorption capacity of the adsorbent. A small hump approximately near around 1105 cm^{-1} represents $S = O$ stretching vibration bond. The band obtained around at 1390 cm^{-1}represents the $C - N$ stretching vibration and the band obtained at 1646 cm^{-1} define the $N = N$the stretch of an azo group of CR. Furthermore, the band around at 3497 represents the $N - H$ stretching vibration band of CR dye [242,265].

6.2.5.3. X-ray photoelectron spectroscopy analysis

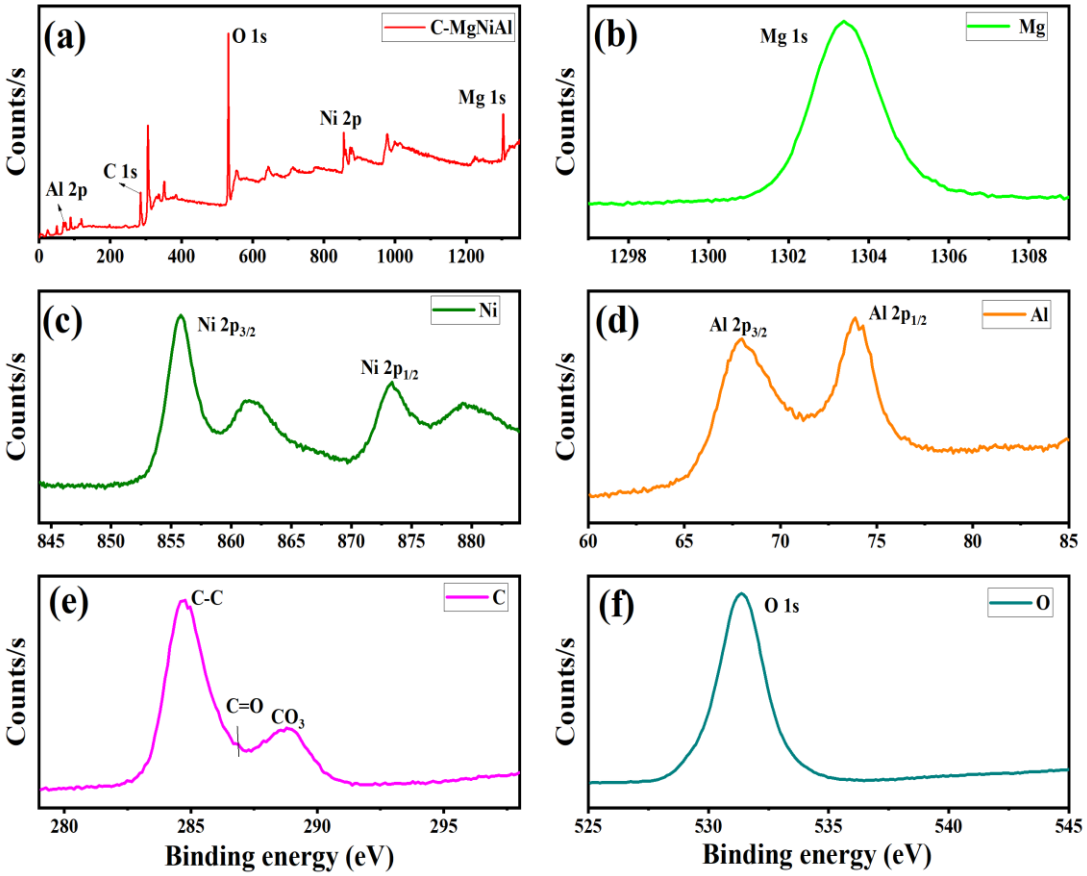

Figure 6.10: XPS spectrum of (a) C-MgNiAl (b) Mg 1s (c) Ni 2p (d) Al 2p (e) C 1s (f) O 1s.

The XPS spectrum of calcined LDH, 9th cycle and 14th cycle after adsorption of CR were investigated for verification of chemical composition and elemental status. In this section, the elements of the materials are shown in Figure 6.10, 6.11 and 6.12. They are mainly composed of Mg, Ni, Al, C and O, respectively, in calcined LDH, and Sulphur is another two materials. The XPS spectrum of 1303.35 eV is an indication of Mg 1s. The high-resolution spectra of Ni 2p give four peaks, which are at 855.71, 861.37, 873.44 and 879.24 eV, respectively. The peak positions at 855.71 and 87.44 eV represent the $Ni\ 2p_{3/2}$ and $Ni\ 2p_{1/2}$ of Ni^{+} in NiO, and the other two are their corresponding satellites, respectively. XPS spectrum of $Al\ 2p$ presents two peaks, which are $Al\ 2p_{3/2}$, $Al\ 2p_{1/2}$ at 67.92 and 73.87 eV for Al_2O_3. The high-resolution spectrum of C1s has shown three peaks. These peaks are at 284.66, 286.89 and 288.92 eV respectively. The first peak corresponds for $C-C$ for surface carbon, the second

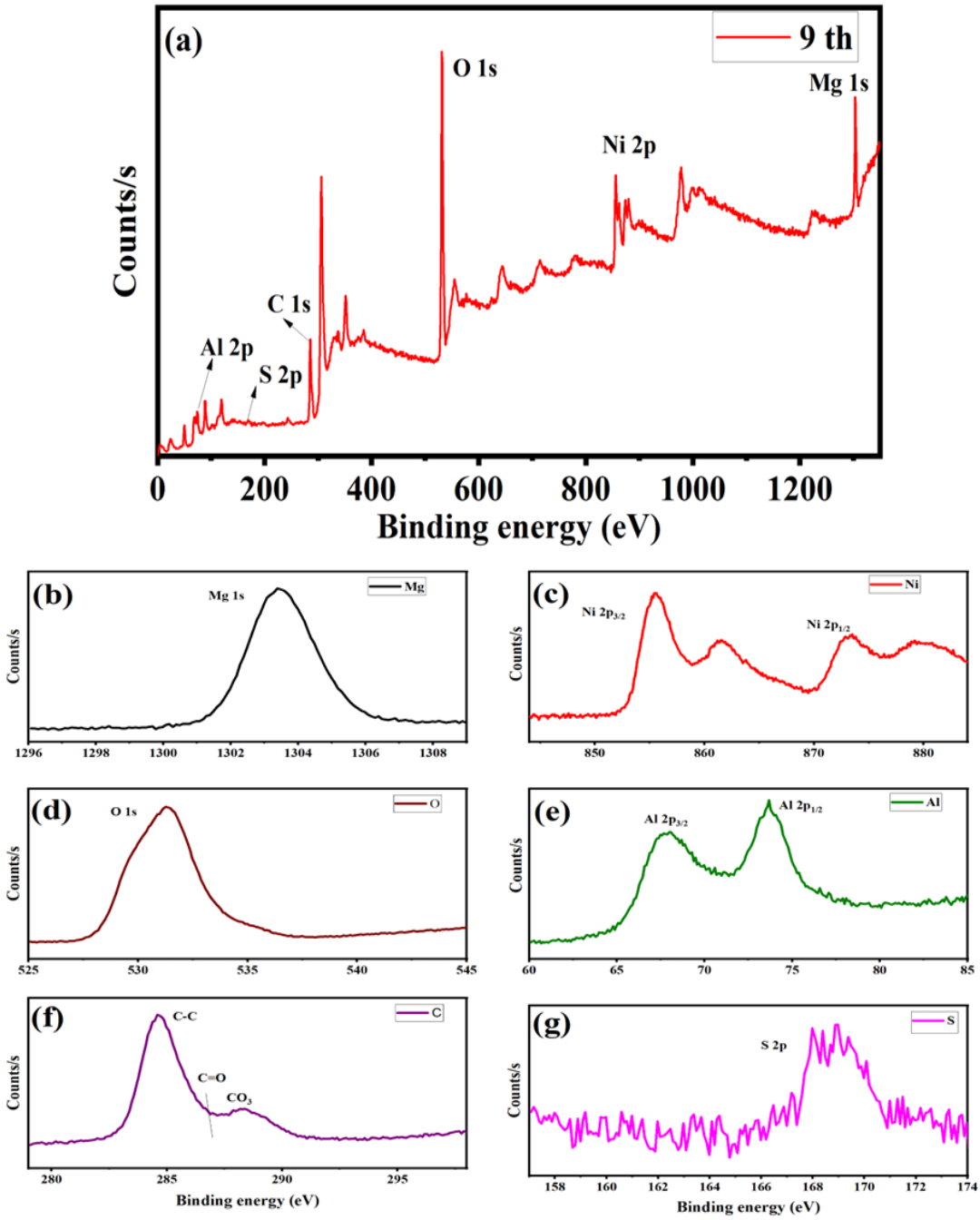

Figure 6.11: XPS spectrum of (a) 9th cycle (b) Mg 1s (c) Ni 2p (d) Al 2p (e) C 1s (f) O 1s (g) S 2p.

peak $C = O$ for adsorbed carbon dioxide coming from the air medium and the last peak is attributed to carbonated species [233]. The XPS spectrum at 168.40 eV indicates S 2p, adsorbed from Congo red, as shown in Figure 11.g and 12.f in the 9th and 14th cycle

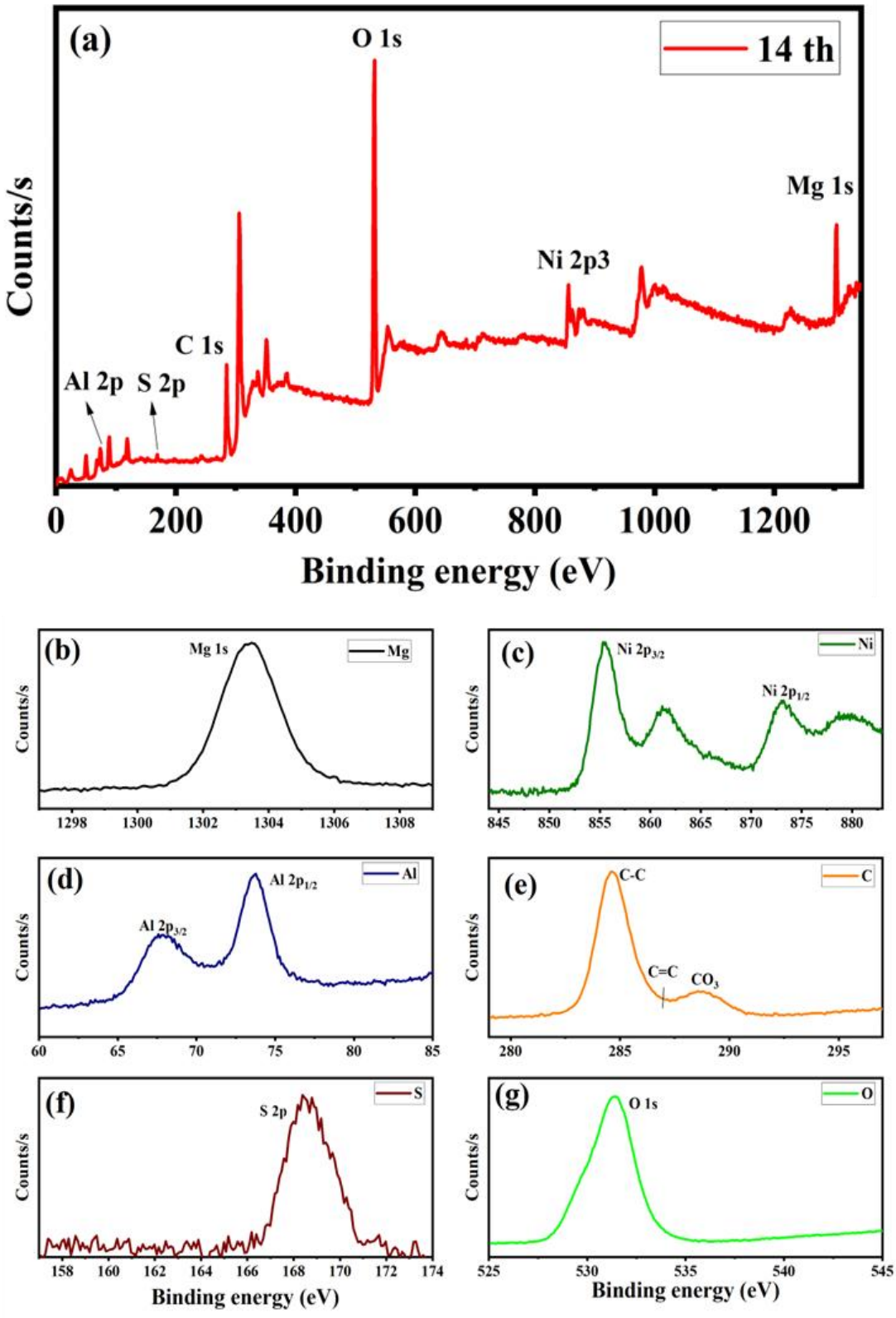

Figure 6.12: XPS spectrum of (a)14th (b) Mg 1s (c) Ni 2p (d) Al 2p (e) C 1s (f) S 2p (g) O 1s.

numbers of the cycle. XPS spectrum of O 1s corresponds to the peak at 531.36 eV, which was coming from an air medium [233,266].

6.2.5.4. Scanning Electron Microscopy analysis of regeneration materials

Figure 6.13 shows the morphological structure of calcined layered double hydroxide after the regeneration of calcined materials. The investigation focused on exploring how the efficiency of calcined materials decreased upon recycling, examining this phenomenon through the morphological alterations observed in the materials. The scanning electron microscope also confirmed the morphological changes. After dye

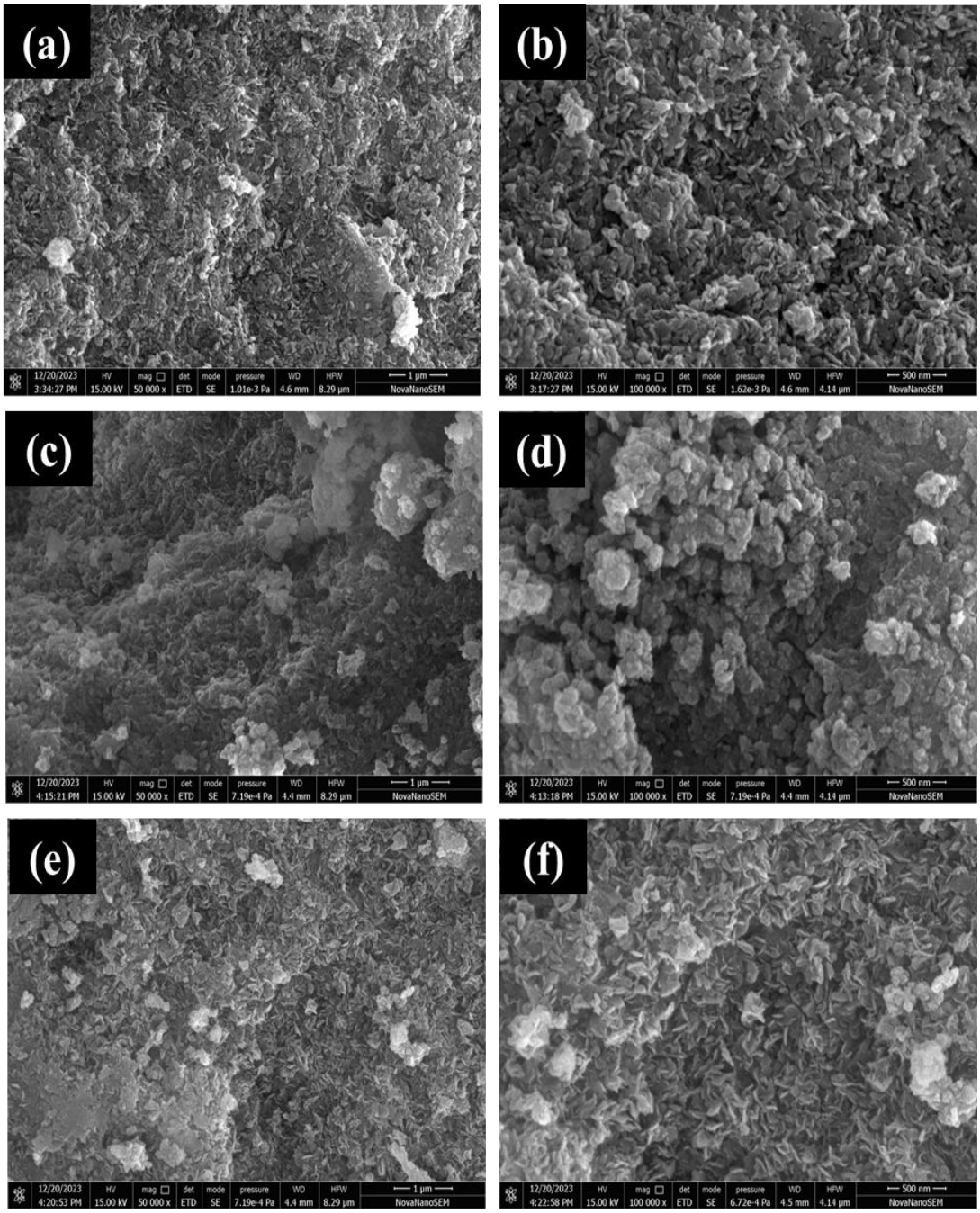

Figure 6.13: SEM images of (a & b) calcined LDH (c & d) 9th cycle CR after adsorption (e & f)14th after after CR adsorption of calcined LDH.

adsorption, the material surface becomes rough and curly with a white layer on the adsorbent surface (SEM image). However, the materials' stability was maintained for a long period of time during the recycling test. In this case, with the increase in recycling, the materials' efficiency gradually declined because the CR dye's sulphonyl group (confirmed by FTIR) was being substituted. The material surface active sites are available to adsorb the anionic dye due to the coulomb attraction force, as the surface charge of LDH is positive and the anionic dye is negative. After the adsorption of the CR dye, the active sites of the material were blocked slowly by the deposition of the sulphur on the surface. The material exhibited remarkable stability until the 9^{th} cycle, after which its efficiency began to decline gradually until the 14^{th} cycle. It will continue operating for an extended period once its effectiveness decreases up to 50%.

The material's reusability for dye removal has proven to be quite promising. During recycling, the initial 9^{th} cycles exhibited exceptional efficiency in dye adsorption, with only a slight decline in performance subsequently. Notably, by the 12^{th} cycle, the efficiency fell below the 90% threshold. However, it remained commendably above 85% even after the 14^{th} cycle. The decline in the material's recyclability may be attributed to the depletion of active sites after repeated restoration, calcination, and adsorption processes. While the X-ray diffraction plot in Figure 6.9a does not indicate the formation of any new phases, it shows a consistent decrease in crystallite size with each successive calcination, which may be due to the reduction of pores leading to a reduction of the total number of active sites for adsorption. Nonetheless, the marginal reduction in crystallite size appears to have a negligible effect on the decrease in dye adsorption. An alternative factor may be responsible for this phenomenon.

In the X-ray Photoelectron Spectroscopy (XPS) analysis, the recycle material's distinctive peak attributed to sulfur 2p orbitals is noticeable. This distinctive S 2p peak was absent in the material before its exposure to adsorption and subsequent recalcination processes. The presence of residual sulphur is likely attributed to the Congo red dye, which, during calcination, contributes to the introduction of sulfur residues, as evident from the increase in intensity of the peak attributed to Sulphur 2p with subsequent cycle. This phenomenon can be explained through the electrostatic interactions between the negatively charged sulphonyl groups within the CR moiety and the positively charged metal layers of the calcined LDH. During adsorption, these sulphonyl groups find a stable electrostatic anchor on the metal layers, forming a strong

binding affinity (the atomic ratio of each compound is shown in Table 6.6). When the desorption process commences, the volatile organic components of the dye are efficiently removed, leaving behind the sulfur residues to accumulate on the calcined material. These sulfur residues possibly obstruct the active sites, contributing to the material's adsorption efficiency decline over repeated cycles. It is reasonable to suggest that these sulfur residues potentially obstruct the active sites, thereby playing a role in the diminishing adsorption efficiency of the material as repeated cycles are conducted. Furthermore, our findings are strengthened by the Fourier Transform Infrared (FTIR) spectra, as depicted in Figure 6.9b, which unmistakably reveal the presence of S=O stretching vibration bonds, providing a direct link to the sulfur compounds introduced during the adsorption and recalcination processes.

Table 6.6. Atomic % of each component during regeneration.

Compound	Sulphur (%)
$C-MgNiAl$	**0**
9^{th} cycle	**0.10**
14^{th} cycle	**0.25**

6.2.6. Economic Analysis

The cost analysis of the wastewater treatment and adsorbent preparation demonstrates the financial feasibility of the adsorbent. The entire cost analysis was performed using the lab scale, but only chemical purchases could be found using the industrial cost basis and supplies from the India-Mart location. The material preparation cost is based on the price of energy and chemicals purchased. The cost of energy used for the material preparation was determined by taking into account the cost of Indian electricity used for the synthesis process, sample heating and drying, as well as the purchasing costs of $Mg(NO_3)_2$, $Ni(NO_3)_2$, $Al(NO_3)_3$, NaOH, Na_2CO_3. The simple estimated cost was calculated for removing the Congo Red (CR) dye from the aqueous solution.

In this section, we solely calculated the estimated adsorption expenses necessary to treat each kiloliter (KL) of wastewater containing a 100 mg/L concentration. An additional expense is acquired for the fifteenth round of adsorption and desorption processes due to our material undergoing a successful fourteen-cycle test with over 80% adsorption efficiency. The cost required for the wastewater treatment and comparison to another

method was shown in Tables 6.7 and 6.8. Our cost analysis used a lab basis, but the industrial basis calculation was far less expensive than the lab. The required adsorption cost by $C-MgNiAl$ is 52 Indian rupees per Kilo of Litter wastewater, respectively. The application of $C-MgNiAl$ for wastewater treatment containing CR can save the adsorption cost compared to the other method and another adsorbent. However, the utilisation of the calcined LDH adsorbent, which can undergo fourteen cycles of recycling, has the potential to substantially reduce the expenses related to adsorption for CR removal from wastewater.

The high adsorption capacity and low preparation cost of calcined LDH support its potential as an effective and low-cost adsorbent for removing wastewater containing Congo Red pollutants.

Table 6.7: Cost analysis for Calcined LDH.

Material Name	Average Adsorption Capacity (mg/g)	Preparation cost (Rs)	Adsorption cost for the 15^{th} cycle. (Rs/KL)
$C-MgNiAl$	480	1882	52

Table 6.8: Effective cost analysis of wastewater treatment with different techniques

Methods	**Operating Cost (US$)**
Adsorption Method	**0.00062/L (This Work)**
Electro Coagulation	0.47/L [267]
Chemical Coagulation	0.2/L [267]
Fenton Oxidation	0.026-0.046/L [268]
Photo-Fenton Oxidation	0.027-0.036/L [268]

6.2.7. Adsorption Mechanism

The main factors behind the dye adsorption mechanism include electrostatic interactions, the formation of hydrogen bonds, ion exchange processes, and the surface area and coordination with metals. All adsorption trials are carried out in normal pH circumstances, meaning that the surface of the adsorbent and the Congo red dye show

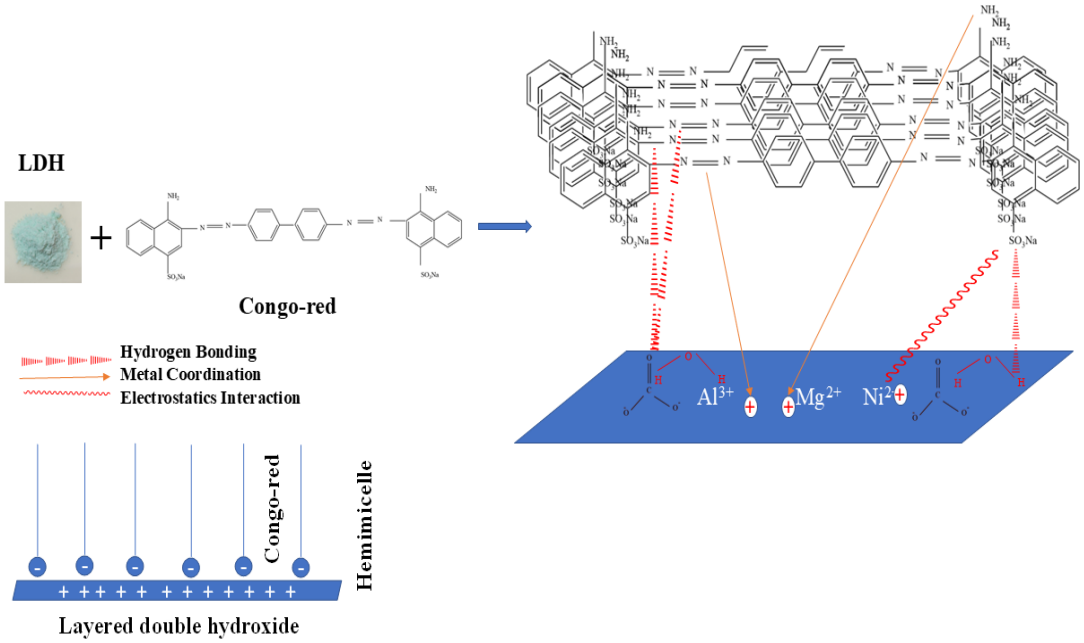

Figure 6.14: Possible mechanism for the adsorption of congo-red on the surface of adsorbent.

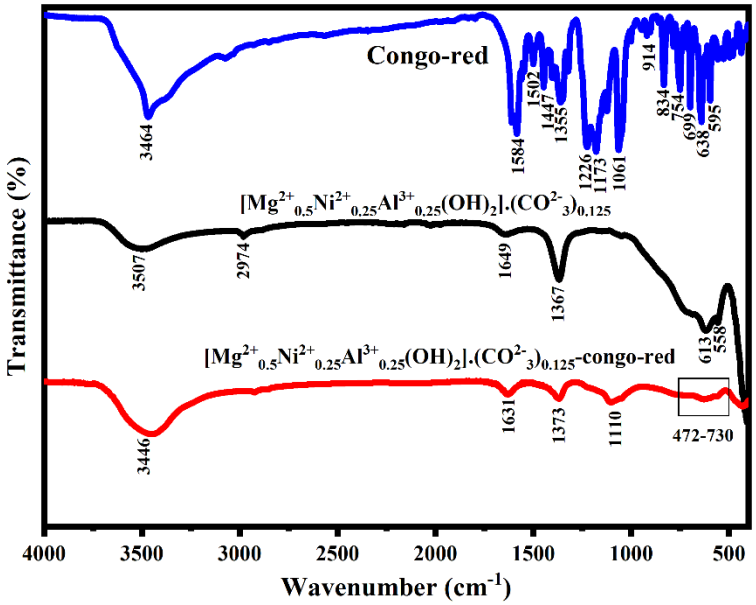

Figure 6.15: FTIR spectra of MgNiAl-CO_3 LDH, congo-red, after adsorption of congo red.

positive and negative charges, respectively. Therefore, electrostatic forces are the main force behind this, while the other interactions are responsible for dye adsorption.

The sulphonyl group (SO_3^{2-}) exhibits on the surface of congo-red dye, which is responsible for the electrostatic forces. This dye has $-NH_2$ group and $-O-$, these are responsible for the hydrogen bonding with surface water on the adsorbent. Congo-red is an azo dye, so it has an azo group ($-N=N-$) and $-NH_2$ group; these make coordination bonds with metals present on the surface of the adsorbent. The adsorption mechanism is similar for the MgNiAl LDH to the report by Arif Chowdhury et al., which involves: (1) The initial adsorption occurs for the material's high surface area and porous nature. (2) increase in the adsorption rate due to monolayer adsorbate formation onto the adsorbent surface by the electrostatics interaction, ion exchange, metal coordination bond and hydrogen bonding, as found in the Langmuir isotherm model. (3) In this region of adsorption, the adsorption process continues until the isoelectric points appear, and the interaction occurs between the adsorbate molecules in the high concentration of dye due to an increase in the diffusion path length. (4) at higher adsorbate concentrations, second layer adsorption begins where individual adsorbed adsorbate molecules behave as an active site, leading to the hemimicelles formation and the adsorption rate increase dramatically. (5) above the critical micelle

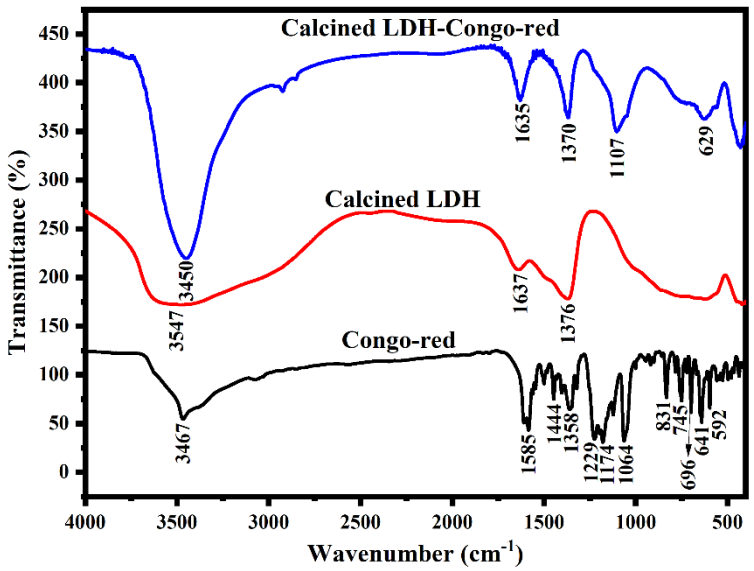

Figure 6.16: FTIR spectra of calcined LDH, congo red, after adsorption of congo red.

concentration, the surface is covered mainly with hemicelles, leading to no further measurable change in the adsorption capacity [269].

In the case of calcined layered double hydroxide, many reasons are reasonable to give remarkable recyclability performance.

(1) Following the calcination process of the layered double hydroxide, a metal oxide is generated because of the heat treatment. The XRD section has already discussed compounds like magnesium and nickel oxide. However, aluminium oxide does not form at low calcination temperatures, so aluminium remains doped with MgO and NiO on the surface of the calcined material. So, Al is available on the surface that is formed a metal coordination bond with $(-\mathrm{N}=\mathrm{N}-)$ and $-NH_2$ group, present in Congo-red. Al is responsible for electrostatic interaction. (2) The surface area is much higher than the layered double hydroxide, and the pore volume is higher, which is helpful for high recyclability. (3) According to W.T. Reichle et al., beyond 700°C, all anions are eliminated. Therefore, this material undergoes calcination at 500°C, where anion exchange interactions occur, accompanied by a small amount of carbonate within the material [270]. (4) In this region of adsorption, the adsorption process continues until the isoelectric points appear, and the interaction occurs between the adsorbate molecules in the high concentration of dye due to an increase in the diffusion path length. (4) at higher adsorbate concentrations, second layer adsorption begins where individual adsorbed adsorbate molecules behave as active sites, leading to the hemimicelles formation and the adsorption rate increase dramatically. (5) above the critical micelle concentration, the surface is largely covered with hemicelles, leading to no further measurable change in the adsorption capacity [269].

To confirm the interaction between the adsorbate and adsorbent, the FTIR has done after the adsorption of the dye molecules for both calcined and uncalcined layered double hydroxide.

In Figure (6.15), $-OH$ ions in layered double hydroxide shift higher wavenumber (3507 cm^{-1}) to lower wavenumber (3446 cm^{-1}) and the peak becomes broad, an indication of involvement for congo-red adsorption. After adsorption of congo-red by the layered double hydroxide, a new peak at 1110 cm^{-1} represents the $S=O$ group, which indicates the layered double hydroxide adsorbs the congo-red.

In Figure (6.16), for calcined layered double hydroxide, wavenumber at 3547 cm^{-1} shifts at lower wavelength 3450 cm^{-1} after adsorption of congo-red. In the calcined layered double hydroxide, wavenumber at 1637 and 1376 cm^{-1} shifts to the lower wavelength at 1635 and 1370 cm^{-1}, which indicates that the calcined layered double hydroxide adsorbs congo-red. After congo-red adsorption, a new one is coming at 1107 cm^{-1}, represents the $S = O$ and a new one at 629 cm^{-1}, which shows the material is involved in congo-red adsorption.

6.2.8. Conclusion

The outcomes of this study indicate that prepared $\mathrm{MgNiAl-CO_3}$, ternary LDH is highly effective for the adsorption of CR and is particularly suitable for removing the anionic dye from wastewater with high concentrations. There is a higher removal of CR by $\mathrm{C-MgNiAl}$ than $\mathrm{MgNiAl-CO_3}$. The pseudo-second-order kinetic model was used to analyse the kinetic data, and the Langmuir isotherm was fitted correctly to the isotherm analysis. Among the different adsorbents available, this one stands out for its high efficiency in removing anionic dye. Based on this comparative study, it is evident that this adsorbent outperforms others, making it a very competitive choice. The substance is inexpensive, requiring only 52 Indian rupees to treat each kiloliter of wastewater. The mesoporous $\mathrm{C-MgNiAl}$ is a promising adsorbent for removing pollutants from wastewater due to its high surface area, unique pore structure, low cost, and highly efficient property with an adsorption equilibrium time of less than 20 min. The highest adsorption capabilities of LDH and calcined LDH are 181.81 and 480.81 mg/g, respectively. Furthermore, the calcined MgNiAl displayed exceptional stability and a remarkable ability to be reused, establishing it as a highly prized material for treating industrial wastewater. The material's reusability for dye removal has proven to be quite promising. During the initial nine cycles, it exhibited exceptional efficiency in dye adsorption, with only a slight decline in performance subsequently. The efficiency fell below the 90% threshold after the 12th cycle. However, it remained commendably above 85% even after the 14th cycle.